Subscriber access provided by the University of Exeter

Article

Dual Stimuli-responsive Block Copolymers with Adjacent Redox- and Photo-cleavable Linkages for Smart Drug Delivery

Yu-Lun Lo, Ming-Fong Tsai, Yugendhar Soorni, Chin Hsu, Zi-Xian Liao, and Li-Fang Wang

Biomacromolecules, **Just Accepted Manuscript** • DOI: 10.1021/acs.biomac.0c00773 • Publication Date (Web): 14 Jul 2020

Downloaded from pubs.acs.org on July 16, 2020

Just Accepted

"Just Accepted" manuscripts have been peer-reviewed and accepted for publication. They are posted online prior to technical editing, formatting for publication and author proofing. The American Chemical Society provides "Just Accepted" as a service to the research community to expedite the dissemination of scientific material as soon as possible after acceptance. "Just Accepted" manuscripts appear in full in PDF format accompanied by an HTML abstract. "Just Accepted" manuscripts have been fully peer reviewed, but should not be considered the official version of record. They are citable by the Digital Object Identifier (DOI®). "Just Accepted" is an optional service offered to authors. Therefore, the "Just Accepted" Web site may not include all articles that will be published in the journal. After a manuscript is technically edited and formatted, it will be removed from the "Just Accepted" Web site and published as an ASAP article. Note that technical editing may introduce minor changes to the manuscript text and/or graphics which could affect content, and all legal disclaimers and ethical guidelines that apply to the journal pertain. ACS cannot be held responsible for errors or consequences arising from the use of information contained in these "Just Accepted" manuscripts.

is published by the American Chemical Society. 1155 Sixteenth Street N.W., Washington, DC 20036

Published by American Chemical Society. Copyright © American Chemical Society. However, no copyright claim is made to original U.S. Government works, or works produced by employees of any Commonwealth realm Crown government in the course of their duties.

Dual Stimuli-responsive Block Copolymers with Adjacent Redox- and Photo-cleavable Linkages for Smart Drug Delivery

Yu-Lun Lo,[a,b#] Ming-Fong Tsai,[a#] Yugendhar Soorni,[a] Chin Hsu,[b] Zi-Xian Liao[c], and Li-Fang Wang*[a,c,d]

[a]Department of Medicinal and Applied Chemistry, College of Life Sciences, Kaohsiung Medical University, Kaohsiung 807, Taiwan

[b]Department of Physiology, Faculty of Medicine, College of Medicine, Kaohsiung Medical University, Kaohsiung 807, Taiwan

[c]Institute of Medical Science and Technology, National Sun Yat-Sen University, Kaohsiung 804, Taiwan

[d]Department of Medical Research, Kaohsiung Medical University Hospital, Kaohsiung 807, Taiwan

Correspondence to: Li-Fang Wang, Professor of Medicinal & Applied Chemistry

College of Life Sciences
Kaohsiung Medical University
100, Shih-Chuan 1st Rd, Kaohsiung City 807, Taiwan
Tel: 011-886-7-3121101-2217
Fax: 011-886-7-3125339
E-mail: lfwang@kmu.edu.tw

Manuscript submitted to Biomacromolecules on May 18, 2020

1st revision on June, 20, 2020

2nd revision on July 9, 2020

ABSTRACT

A novel dual-stimuli cleavable linker containing adjacent UV light-sensitive *o*-nitrobenzyl ester (ONB) and GSH-responsive disulfide bonds was first designed and synthesized to increase the responsivity to external stimuli. The functionalized linker was then utilized to prepare a dual-responsive amphiphilic block copolymer using ring opening polymerization and atom transfer radical polymerization. The copolymer formed a micelle in an aqueous solution and showed dual-stimuli responses including photo-mediated cleavage under UV light irradiation at 365 nm as well as reduction-responsive degradation in the presence of a reducing agent. The micelle was nontoxic against three cell lines and majorly internalized via clathrin-mediated endocytosis. Doxorubicin (Dox) was loaded in the hydrophobic core of the micelle. Enhancement of a cell-killing effect against A549 cells was clearly observed in the Dox-encapsulated micelle when exposed to UV light.

Keywords: micelle, dual-stimuli response, ring opening polymerization, atom transfer radical polymerization, clathrin-mediated endocytosis, doxorubicin

■ INTRODUCTION

Stimuli-responsive amphiphilic block copolymers have been extensively studied with respect to biomedical applications because of their tremendous responsiveness to external triggers such as light, pH, redox, ultrasound, and ionic forces.[1] Integration of different kinds of the stimuli-reactive linkers into a block copolymer can be achieved by designing dual or multi stimuli-responsive compartments either as pendent groups or in the backbone chain of parent block copolymers.[2] The main goal of all designs is to induce polymeric micelles to undergo efficient and controllable degradation upon external stimuli and consequently, encapsulated agents in the hydrophobic domain of polymeric micelles can be efficiently released at a target tissue on-demand.[3]

Among external physical stimuli, a photo-mediated therapy strategy is attractive because light can direct active molecules into targeted site in highly spatiotemporal precision under light irradiation at a specific wavelength. In addition, it is noninvasive and shows minimal toxicity to normal tissue.[4] Light-cleavable moieties include organic coumarin, 3′, 5′-di(carboxymethoxy) benzoin acetate and *o*-nitrobenzyl (ONB) derivatives and inorganic (Ru, Pt, and Mn complexes) compounds, undergoing an irreversible reaction.[5] Although an organic ONB family is widely developed for drug

delivery applications,[6-8] nevertheless, it has some drawbacks. For example, the release rates of the ONB family are slower than those of coumarin derivatives.[9] After irradiation, the produced fragment (i.e. nitrosoaldehyde) can react with amines to form imine bonds, which can especially be a problem for abundance of surrounding proteins in living tissues.[10]

Glutathione (GSH) is a thiol-containing tripeptide, showing different concentrations in intracellular (1 - 10 mM) and extracellular areas (2 - 20 μM) in living cells.[11] The cytosolic GSH concentrations in cancer cells are several times higher than those in normal cells.[12] Thus, the use of GSH concentration gradient is a promising approach to respond to the tumor microenvironment (TME) and to control therapeutics released at the tumor site. The combination of a redox-cleavable disulfide linkage and a photo-cleavable ONB linkage has been widely reported in several polymers[13-15] and hydrogel[16] to demonstrate the dual-responsive behavior; however, the disulfide and ONB linkages are positioned at different places of the polymeric structures. We speculate such designs might need a higher concentration of reducing agents or longer time exposed to light than those placing two responsive linkages together.

Herein, a novel dual-stimuli cleavable linker containing adjacent UV light-sensitive ONB ester and GSH-responsive disulfide bonds, 2-(2-(2-bromo-2-methylpropanoyl) oxy ethyl disulfanyl) ethyl 4-(hydroxymethyl)-3-nitrobenzoate (OH-ONB-SS-Br) is first designed and synthesized to increase the responsivity to the external stimuli. This functionalized linker is utilized to prepare a dual-responsive amphiphilic block copolymer using ring opening polymerization (ROP) and atom transfer radical polymerization (ATRP). The synthesized dual-stimuli cleavable linker is located between the hydrophobic and hydrophilic junctions of the amphiphilic copolymer in which the ONB ester moiety undergoes photolysis under UV light irradiation and the disulfide linkage can be dissipated by reducing agents like dithiothreitol (DTT) or GSH.[13, 17-19] Similar degradation fragments will be formed either with the presence of a reducing agent or under light irradiation. The dual-stimuli responsive cleavage may decrease the required amount of ONB and simultaneously solve the aforementioned disadvantage of ONB; additionally, the GSH-responsible behavior has the merit of increasing the drug release at the tumour site. Here, the artificially-made amphiphilic block copolymer will be well-characterized and its responsiveness to the external stimuli will be thoroughly assayed to demonstrate the success of the design.

■ EXPERIMENTAL SECTION

Materials. 4-Bromomethyl-3-nitrobenzoic acid, sodium carbonate (Na_2CO_3), *p*-toluenesulfonic acid (*p*TSA), 3,4-dihydro-2H-pyran (dihydropyran), 2-bromo-2-methylpropionyl bromide, triethylamine (TEA), N,N'-dicyclohexylcarbodiimide (DCC), 4-dimethylaminopyridine (DMAP), tin(II) 2-ethylhexanoate ($Sn(Oct)_2$) copper(I) bromide (CuBr), and trifluoroacetic acid (TFA) were purchased from Alfa Aesar. 4-(Bromomethyl)-3-nitrobenzoic acid, ε-caprolactone (CL), *tert*butyl methacrylate (*t*BMA), N,N,N',N",N"-pentamethyldiethylenetriamine (PMDETA), (1-ethyl-3-(3-dimethyl aminopropyl) carbodiimide hydrochloride) (EDC), and N-hydroxysuccinimide (NHS) were purchased from Sigma-Aldrich. 3-(4,5-Dimethylthiazol-2-yl)-2,5-diphenyl-tetrazolium bromide (MTT) was from MP Biomedicals. Phosphate buffer saline (PBS), Dulbecco's Modified Eagle Medium (DMEM), Roswell Park Memorial Institute (RPMI) 1640 Medium, trypsin–EDTA and fetal bovine serum (FBS) were purchased from Invitrogen. Doxorubicin (Dox) was purchased from Combi-Blocks.

Synthesis of OH-ONB-SS-Br Macroinitiator (6)

*Synthesis of 4-(Hydroxymethyl)-3-nitrobenzoic Acid (**2**).* The reaction procedure of OH-

ONB-SS-Br macroinitiator is shown in Scheme 1. To synthesize compound **2**, the solution containing 4-(bromomethyl)-3-nitrobenzoic acid (5.00 g, 19.23 mmol) and Na_2CO_3 (7.13 g, 67.30 mmol) in water: acetone (1:1 v/v, 150 mL) was refluxed at room temperature (RT) for 5 h and purified according to the literature.[22] The compound **2** is a pale brown solid (3.5 g, 94.6% yield). ^{1}H-NMR (200 MHz, DMSO-d_6, ppm) 8.58 (s, 1H, –CH–Phenyl.–), 8.37 (d, 1H, –CH–Phenyl.–), 8.03 (d, 1H, –CH–Phenyl.–), 5.75 (t, 1H, OH–CH_2–Phenyl.–), 4.97 (d, 2H, OH–CH_2–Phenyl.–). MS (ESI) *m/z* calcd for $C_8H_7NO_5$: 197.0; found: 195.97 $[M-1]^+$.

*Synthesis of 2-(2-Hydroxyethyl-disulfanyl) ethyl-2-bromo-2-methylpropanoate (HO-SS-Br) (**3a**).* The HO-SS-Br was synthesized according to the literature.[20] Briefly, the solution consisting of bis(2-hydroxyethyl) disulfide (5.00 g, 32.4 mmol) and TEA (12.0 mL, 86.1 mmol) in THF was stirred at RT for 20 min under an argon atmosphere. The compound **3a** is a pale yellowish liquid (4.0 g, 40.8% yield). ^{1}H-NMR (200 MHz, $CDCl_3$, ppm) 4.45 (t, 2H, –CH_2OC (O)–), 3.90 (t, 2H, HO–CH_2–), 3.00 (t, 2H, –SS–CH_2—), 2.90 (t, 2H, (–CH_2–SS–), 1.95 (s, 6H, –C(CH_3)$_2$Br). MS (ESI) *m/z* calcd for $C_8H_{15}BrO_3S_2$: 302.0; found: 303.93 $[M+1]^+$.

*Synthesis of 3-Nitro-4-((tetrahydro-2H-pyran-2-yl) oxy methyl) Benzoic Acid (THP-ONB-COOH) (**4**).* 4-(Hydroxymethyl)-3-nitrobenzoic acid (5.00 g, 25.4 mmol) and *p*TSA (0.021 g, 0.12 mmol) were dissolved in THF (50 mL) and the mixture was stirred at RT for 15 min. Under an argon condition, 4.05 mL of 3, 4-dihydro-2H-pyran was dropwise added to the mixture and refluxed for 10 h. After the solvent was removed by rotary evaporator,

the residue was purified by column chromatography (silica gel 75-200 mesh) using 10% EA: petroleum ether mobile phase to yield a pale yellow solid of **4** (7.0 g, 98.6% yield). ^{1}H-NMR (200 MHz, DMSO-d_6, ppm) 8.80 (s, 1H, –CH-Phenyl.–), 8.37 (d, 1H, –CH-Phenyl.–), 8.00 (d, 1H, –CH-Phenyl.–), 5.30 – 4.95 (m, 2H, –O–CH_2–Phenyl.–), 4.80 (s, 1H, –O–CH–O–) 3.95 – 3.80 (m, 2H, –C–CH_2–C–), 3.70 – 3.50 (m, 2H, –C–CH_2–C–), 2.00 – 1.77 (m, 2H, –C–CH_2–C–), 1.70 – 1.50 (m, 2H, –C–CH_2–C–). MS (ESI) *m/z* calcd for $C_{13}H_{15}NO_6$: 281.1; found: 279.90 $[M-1]^+$.

*Synthesis of 2-(2-(2-Bromo-2-methylpropanoyl) oxy ethyl disulfanyl ethyl-3-nitro-4-(tetrahydro-2H-pyran-2-yl) oxy methyl) Benzoate (THP-ONB-SS-Br) (**5**).* 3-Nitro-4-((tetrahydro-2H-pyran-2-yl)oxy methyl) benzoic acid (5.00 g, 17.8 mmol) and 2-(2-hydroxyethyl-disulfanyl) ethyl-2-bromo-2-methylpropanoate (6.40 g, 21.3 mmol) were mixed in DCM (100 mL). Under an argon atmosphere, DMAP (0.43 g, 3.55 mmol) and DCC (1.80 g, 8.88 mmol) were added, and the mixture was stirred at RT for 16 h. After complete reaction, the residue was purified by column chromatography using 5% EA: petroleum ether mobile phase to yield a yellowish green liquid of **5** (6.5 g, 65.0% yield). ^{1}H-NMR (200 MHz, $CDCl_3$, ppm) 8.70 (s, 1H, –CH-Phenyl.–), 8.30 (d, 1H, –CH-Phenyl.–), 7.95 (d, 1H, –CH-Phenyl.–), 5.30 – 4.90 (m, 2H, –O–CH_2–Phenyl.–), 4.80 (s, 1H, –O–CH–O–), 4.70 (t, 2H, –CH_2OC (O)–), 4.50 (t, 2H, –CH_2OC (O)–), 3.97 – 3.80 (m, 2H, –C–

CH_2–C–), 3.65 – 3.50 (m, 2H, –C–CH_2–C–), 3.95 – 2.95 (m, 4H, –SS–CH_2–CH_2OC (O)–), 2.00 (s, 6H, –O=C–$(CH_3)_2$–Br–), 1.90 – 1.70 (m, 2H, –C–CH_2–C–), 1.65 – 1.50 (m, 2H, –C–CH_2–C–).

*Synthesis of 2-(2-(2-Bromo-2-methylpropanoyl) oxy ethyl disulfanyl) ethyl 4-(hydroxymethyl)-3-nitrobenzoate (OH-ONB-SS-Br) (**6**).* Compound **5** (5.00 g, 8.82 mmol) was put into a clean round bottom flask and dissolved in THF (40 mL). Under an argon atmosphere, *p*TSA (0.021 g, 0.12 mmol) was added to the mixture and stirred at RT for 18 h. The column chromatography was utilized to purify the residue with 10% EA: petroleum ether mobile phase to yield a pale green liquid of **6** (2.5 g, 59.5% yield). ^{1}H-NMR (200 MHz, $CDCl_3$, ppm) 8.75 (s, 1H, –CH-Phenyl.–), 8.35 (d, 1H, –CH-Phenyl.–), 7.95 (d, 1H, –CH-Phenyl.–), 5.15 (d, 2H, HO–CH_2–Phenyl.–), 4.65 (t, 2H, –CH_2OC (O)–), 4.45 (t, 2H, –CH_2OC (O)–), 3.95 – 2.95 (m, 4H, –SS–CH_2–CH_2OC (O)–), 2.00 (s, 6H, –O=C–$(CH_3)_2$–Br–). MS (ESI) *m/z* calcd for $C_8H_{15}BrO_3S_2$: 481.0; found: 481.80 $[M]^+$.

Synthesis of PCL-ONB-SS-PMAA Diblock Copolymer

Synthesis of Poly(ε-caprolactone)-ONB-b-bromide with a Disulfide Linkage (PCL-ONB-SS-Br). The PCL-ONB-SS-Br was synthesized under an argon atmosphere using HO-ONB-SS-Br (96 mg, 0.31 mmol), CL (2.19 mL, 19.5 mmol), $Sn(Oct)_2$ (15.9 mg, 0.049 mmol) and toluene (2.1 mL). The ROP was carried out at 120 °C for 6 h in a glove box,

and the PCL-ONB-SS-Br was purified according to previous publication.[21]

Synthesis of PCL-ONB-SS-PMAA. The asymmetric diblock copolymer of PCL-ONB-SS-P*t*BMA was synthesized by ATRP using PCL-ONB-SS-Br (200 mg, 0.028 mmol), CuBr (12.3 mg, 0.085 mmol), PMDETA (21.0 mg, 0.091 mmol), *t*BMA (617 mg, 4.34 mmol) and toluene (1.5 mL) in a round-bottom flask. The flask was degassed by consecutive standard freeze–pump–thaw cycles for three times. The ATRP was carried out at 50 °C for 6 h in the glove box. The *tert*-butyl ester groups of PCL-ONB-SS-P*t*BMA were removed in an acid condition of TFA to yield PCL-ONB-SS-PMAA according to previous publication.[21]

Characterization of Block Copolymer. ^{1}H-nuclear magnetic resonance (^{1}H-NMR) spectra were recorded on a Varian Gemini (200 MHz) NMR spectrometer using $CDCl_3$ or DMSO-d_6 as a solvent to determine chemical structures. Gel permeation chromatography (GPC) was acquired to determine molecular weights (MW) using an Agilent 1200 series equipped with a Shodex-KF804L and KF-803 connected column. FT-IR spectrum was acquired from Bruker ALPHA-T spectrometer. Mass data was acquired from TRACEGC-POLARISQ (Thermo Finnigan) and Waters ZQ 4000 mass spectrometer.

Preparation and Characterization of Micelles

Micelle Formation. A dialysis method was acquired for preparation of PCL-ONB-SS-PMAA micelle ($POSP_m$). The morphologies of $POSP_m$ were observed by transmission electron microscope (TEM HT7700, Hitachi), and the size distribution of $POSP_m$ was measured by dynamic light scattering (DLS) zeta-sizer (ELSZ-2000, Otsuka Electronics). The critical aggregation concentrations (CAC) of $POSP_m$ were determined using a Cary Eclipse fluorescence spectrophotometer (Varian) with pyrene as a probe according to previous publication.[21]

Reductive- and Photo-triggered Cleavage of $POSP_m$. Redox-driven cleavage of the disulfide linkage of $POSP_m$ was carried out with 10 mM GSH for 20 min. $POSP_m$ was dispersed in DD water containing GSH at 0.5 mg/mL. For photo-triggered cleavage of $POSP_m$, two millimeters of $POSP_m$ aqueous solution were placed into a cuvette (Hellma) and stirred continuously. The cuvette was kept in the dark and irradiated by continuous wave (CW) UV laser diode (365 nm, max. 430 mW/cm^2, TANYU) horizontally under continuous stirring for 20 min. Following reductive- and photo-triggered treatments, the change in size and morphology of $POSP_m$ was observed by DLS and TEM respectively.

Dox-encapsulated $POSP_m$ ($POSP_m$@Dox) and Dox Release. The Dox·HCl powder was dissolved in DMSO at a concentration of 2 mg/mL and an equimolar amount of TEA was added for desalting. One mL of the Dox solution was added into the solution containing 20 mg of the PCL-ONB-SS-PMAA copolymer in 4 mL of DMSO.[29] A dried sample of $POSP_m$@Dox was dissolved in DMSO at a concentration of 1 mg/mL, and the Dox content

was calculated against a calibration curve using a UV-Vis spectrometer (Agilent 8453) at the wavelength of 485 nm. The loading efficiency (LE) and encapsulation efficiency (EE) were reported as follows.

LE (%) = (amount of drug in micelle / total amount of $POSP_m$@Dox) x 100 (1)

EE (%) = (amount of drug in micelle / amount of drug in feed) x 100 (2)

The redox- and photo-trigger-released behavior of Dox from $POSP_m$@Dox was determined in PBS at pH 7.4 and 37 °C for simulating a physiological condition. The 800 μ L of $POSP_m$@Dox solution at 3 mg/mL was put in a DiaEasy™ Dialyzer (MWCO 3.5kDa, BioVision) and immersed in 10 mL of PBS (1) for whole time (control), (2) for 6 h, followed by treatment with 10 mM GSH, (3) for 6 h, followed by treatment with UV irradiation for 20 min, (4) for 6 h, followed by treatment with 10 mM GSH and UV irradiation for 20 min. At a certain time interval, one mL of PBS solution was carefully removed from the tube and replaced with 1 mL of fresh PBS to maintain a sink condition. Besides being irradiated at the time point of 6 h, groups 3 and 4 were also treated with light irradiation for 20 min at another two time points of 12 and 24 h. The Dox concentration was determined using an UV−vis spectrophotometer as aforementioned.

Cell Experiments

Cell Culture. Non-small cell lung carcinoma A549 cells were cultured in RPMI, and human normal lung fibroblasts HEL-299 cells and non-small cell lung carcinoma CRL-5802 cells were cultured in DMEM, respectively containing 10% fetal bovine serum (FBS) and 100 μg/mL penicillin/streptomycin in a 37°C incubator with a humidified atmosphere

containing 5% CO_2.

Relative Cell Viability of $POSP_m$ Micelle and $POSP_m$@Dox Micelle. The cell viability of $POSP_m$ was determined with an MTT assay against A549 cells, CRL-5802 cells and HEL-299 cells according to previous publication.[28] The cytotoxic efficacy of $POSP_m$@Dox was done in A549 cells alone. To test the photo-triggered cytotoxicity of $POSP_m$@Dox, A549 cells were seeded into 12 well plates (1×10^5 cells/well) for 24 h and added with an equivalent concentration of free Dox or $POSP_m$@Dox at 2 μg/mL. Following 4 h incubation, the medium was replaced with 1 mL of fresh complete medium, and the cells were exposed to UV light (365 nm, 430 mW/cm^2) for 20 min and postincubated for another 48 h. The cytotoxic efficacy of $POSP_m$@Dox and free Dox was determined with the MTT assay.

Endocytosis Pathway of Micelle. Rhodamine 123 (R123) was conjugated with $POSP_m$ by EDC/NHS coupling reaction to examine the internalization pathway of $POSP_m$ into A549 cells.[21] A549 cells (2×10^5 cells/well) were seeded in 6-well plates and incubated for 24 h. The cells were pretreated with inhibitors: chlorpromazine (10 μg/mL), wortamannin (50 nM), genistein (200 μM), separately for 30 min and analyzed by flow cytometry.[28]

The intracellular uptake of $POSP_m$@Dox was also observed with a confocal laser

scanning microscope (CLSM, LSM 700 Zeiss Confocal Microscopy). A549 cells (1.0×10^5 cells/well) were seeded in 12-well plates with one sterilized glass coverslip/well for 24 h, and the cells were treated as same as aforementioned in the MTT assay. The fluorescence intensity was analyzed by MetaVue software. The Annexin-V/PI (propidium iodide) dual staining assay was performed to estimate apoptosis-inducing efficacy of free Dox, $POSP_m$@Dox before and after UV light irradiation as well.[29]

Statistical Analysis. Experiments were repeated at least three times, and data are expressed as the mean ± standard deviation. Student's t-test was performed to determine the statistical significance of the respective group. *$p < 0.05$ or **$p < 0.01$ indicated a significant difference.

■ RESULTS AND DISCUSSION

Copolymer Synthesis and Characterization. The synthetic approach of PCL-ONB-SS-PMAA was associated with eight steps (Scheme 1). Initially, compound **2** with the ONB moiety was synthesized according to the procedure reported[22] and the ^{1}H-NMR and LC/MS spectra of compound **2** are in good consistency (Supporting Information Figs. 1Sa & 1Sb). Secondly, the benzyl hydroxyl group was protected

with 3,6-dihydro-2H-pyran to yield compound **4** (Supporting Information Figs. S1c & S1d) and proceeded for further esterification process with compound **3a** (Supporting Information Figs. S1e & S1f) to yield compound **5**. The ^{1}H-NMR spectrum of compound **5** is shown in Figure 1a. Compound **5** was de-protected with p-TSA to obtain compound **6** (macroinitiator) containing hydroxyl (-OH) group on one end and tertiary bromide on the other end. Compound **6** was applicable for ROP and ATRP respectively. The ^{1}H-NMR and LC/MS spectra of the compound **6** are shown in Figures 1b & 1c. Thirdly, the ε-caprolactone monomer was used to synthesize compound **8** using $Sn(Oct)_2$ as a catalyst through ROP. The ^{1}H-NMR spectrum of PCL-ONB-SS-Br (compound **8**) is shown in Figure 2a. In the further step, compound **10** was synthesized using the compound **8**, CuBr and PMDETA via ATRP. Following the reaction, the polymer solution was dissolved in THF and passed through the neutral alumina to remove the residual Cu^{+} ion. The ^{1}H-NMR spectrum of PCL-ONB-SS-P*t*BMA (compound **10**) is shown in Figure 2b and the increase in MW before and after ATRP was measured by GPC as shown in Figure 2c. The *tert*-butyl moieties of the ester groups were removed into carboxylic acid groups upon treating the copolymer solution with TFA to obtain compound **11**, where the carboxylic acid proton peak appears ~12.4 ppm in ^{1}H-NMR spectrum

(Figure 2d).

In light of the literature review,[23-26] the ONB ether linkage is commonly used to make the copolymers containing ONB moiety instead of ONB ester linkage. Thus, we initially designed and synthesized an ONB ether linkage between the junction of PMAA and PCL (Supporting Information Scheme S1). However, a shoulder peak was observed at ~15 min elution time in a GPC profile (Supporting Information Fig. S2a). This shoulder peak always existed in GPC profiles even though the reaction time was prolonged to 12 h (Supporting Information Fig. S2b). We speculated that the ONB ether linkage was unstable as the ROP reaction was carried out at a high temperature of 90 ^{o}C. The ONB ether linkage degraded and formed a fragmented PCL-ONB-OH structure as indicated in Fig. S2a. The positive inductive effect of methyl groups on aromatic ether position of the polymer containing ONB ether linkage accelerated the disintegration of the ether linkage[27] and thus converted it into hydrophobic polymer fragments bearing phenolic -OH group (PCL-ONB-OH), which was not applicable for further ATRP reaction. Hence, we utilized the ONB ester as the macroinitiator for further diblock copolymer synthesis and intended to make the copolymer more stable towards temperature and mild acidic conditions.

Micellar Formulation and Drug Encapsulation. A dialysis method was adopted to

prepare a PCL-ONB-SS-PMAA micelle ($POSP_m$). The CAC values of $POSP_m$ were determined using a fluorescence pyrene as the probe, i.e. 1.18 x 10^{-2} mg/mL at pH 5.5 and 8.25 x 10^{-3} mg/mL at pH 7.4 respectively (Supporting Information Fig. S3). The low CAC value implied good stability in the physiological condition of pH 7.4.

Scheme 2 depicts photo- and redox-stimuli responsive segments of $POSP_m$. The nitro group present on the benzene ring at *ortho* position undergoes homolysis, and causes the degradation of the ester bond when it absorbs the UV light as a proposed mechanism shown in Scheme 2. In this process, two fragments were formed after UV irradiation, leading to the formation of an *o*-nitrosobenzaldehyde group attached on PMAA segment and a carboxylic acid group attached on the end of PCL segment. An aldehyde signal peak clearly appeared at ~10.2 ppm in the NMR spectrum of the PCL-ONB-SS-PMAA block copolymer in d_6-DMSO after UV irradiation at 365 nm (430 mW/cm^2) for 20 min (Supporting Information Fig. S4). Additional evidence for photo- and redox-responsive characteristics of the block copolymer was confirmed by GPC (Figure 3). PCL-ONB-SS-P*t*BMA was utilized for testing because of the insolubility of PCL-ONB-SS-PMAA in THF. A mono MW distribution of the block copolymer was observed at initiation; nevertheless, a bimodal distribution profile appeared when the copolymer was treated with DTT (50 mM in THF) at a regular time interval. An increase

in MW distribution appearing at longer elution time went hand-in-hand with a decrease in MW distribution appearing at a shorter elution time, indicating the gradual cleavage of the disulfide linkage of the block copolymer (Figure 3a). A similar trend of the MW change of PCL-ONB-SS-P*t*BMA was observed in GPC profiles under UV light irradiation (Figure 3b). These results reconfirmed that the block copolymer underwent a characteristic *o*-nitrobenzyl cleavage when the polymer was irradiated by UV light.

The morphological change of $POSP_m$ was acquired by TEM. The particle size of $POSP_m$ is ~ 80 nm estimated from the TEM image (Figure 4a). Irregular shapes were observed when the micelle was treated with 10 mM GSH for 20 min, UV light irradiation for 20 min, and both combined (Supporting Information Fig. S5a-c), indicating the micelle disintegrated because of the cleavage of the disulfide linkage as well as the ONB moiety.

In parallel, the hydrodynamic size of the micelle was determined to be ~120 nm and the size distribution became broader and broader with time when $POSP_m$ was treated with GSH (Figure 4b). A bimodal size distribution appeared under UV light irradiation and shifted to the large size distribution when the micelle was treated with both stimuli. From GPC, TEM and DLS results, it seemed that the response of $POSP_m$ degradation under UV light irradiation was superior to GSH stimulus. A similar finding has been reported in a

dual-stimuli-responsive ABA-type triblock copolymer micelle, where *o*-nitrobenzyl and disulfide groups were positioned separately in the hydrophobic middle block.[15] A burst release of a hydrophobic drug from disintegrated micelles was traced by UV light but a slow release was followed in the presence of a reducing agent.

***In Vitro* Cytotoxicity and Cellular Uptake Pathway.** The human lung carcinoma cell lines CRL-5802, HEL-299 and A549 cells were cultured in a DMEM or RPMI medium. The cells containing different micellar concentrations within 0–200 μg/mL were added to each well and further incubated for another 24 h under 5% CO_2 at 37 ^{o}C.[28] No obvious cytotoxicity of the cells exposed to the micelle was found at the test concentrations, and their viabilities were still >95% at the highest concentration of 200 μg/mL. The cytotoxicity of the micelle was independent on the cell lines used (Figure 5a).

The cellular uptake of the micelle was tested in CRL-5802 and A549 cells using a flow cytometer, where the internalization of the micelle was higher in A549 cells than in CRL-5802 cells because of the larger right shift in fluorescence intensity (Figure 5b). Three commonly-used chemical inhibitors were adopted for testing the internalization pathway of the micelle into the cells using wortmannin for

micropinocytosis, chlorpromazine for clathrin-mediated endocytosis (CME) and genistein for caveolae-mediated endocytosis.[29] Flow cytometric histograms showed a left shift when A549 cells and CRL-5802 cells were pretreated with chlorpromazine, indicating an inhibition effect and no shifts when the cells were pretreated with genistein and wortmannin. This fact implied that CME is the major internalization pathway. The endocytic pathway highly determined the intracellular destination of nanoparticles (NPs). CME seemed the most promising pathway for cellular entry in drug delivery systems because the drug could be released rapidly from drug-encapsulated NPs.[30-34]

Encapsulation of DOX into $POSP_m$ ($POSP_m$@Dox) and its Cytotoxicity. A micelle has the capability to encapsulate lipophilic agents inside the hydrophobic core for smart drug delivery. The desalt form of doxorubicin (Dox) was used as a hydrophobic drug model, and the Dox calibration curve was established to calculate LE and EE of the drug, i.e. ~7.0% and 75.6% respectively. The *in vitro* Dox released from the micelle was performed in PBS of pH 7.4 to simulate the physiological condition. Initially, four groups of the test samples were immersed in PBS of pH 7.4 for 6 h. About 17% of Dox was gradually released as shown in Figure 6a. After that, the samples in DiaEasy™ Dialyzer containing $POSP_m$@Dox were continually dialyzed against 10 mL of PBS at pH 7.4 and

separately treated with (1) nothing (control), (2) 10 mM GSH, (3) UV irradiation for 20 min, and (4) both 10 mM GSH and UV irradiation for 20 min. After the time point of 6 h, the drug release rate was in the order of Group (4) > Group (3) ≈ Group (2) > Group (1).

Because the difference of drug release profiles among groups was insignificant, another light irradiation was applied at 12 h and 24 h. In Group 4, the drug release percentage clearly increased at 12 h and was larger than those in Groups 2 and 3, and then significantly increased at 24 h, ~20% increase in Dox release. Groups 2 and 3 showed similar release profiles. As depicted in Scheme 2, the micelle might preserve the hydrophobic core and the encapsulated drug gradually becomes released with a single stimulus. In contrast, the micelle disintegrated upon two stimuli and the drug was rapidly released. The combination of redox-responsive disulfide along with the UV-sensitive linkage in the copolymer clearly enhanced disintegration of the micelle in the physiological condition, where the concentration of GSH (3 - 10 mM) was found to be higher than extracellular areas (~ 2.8 μM) in living cells.[35, 36] This fact benefits an effective cellular-triggered drug release because of the cleavage of disulfide linkages in the micelle via disulfide-thiol exchange reactions.[22]

The cytotoxicity of $POSP_m$@Dox was tested against A549 cells (Figure 6b). For 24 h postincubation, the relative cell viability was still > 70% at a high Dox concentration of

20 μg/mL. For 48 h postincubation, the IC_{50} values (the concentration of Dox to inhibit 50% of cell viability) were 1.65 μg/mL for $POSP_m$@Dox and 1.50 μg/mL for free Dox. The potency of $POSP_m$@Dox in induced apoptosis was similar to that of free Dox against A549 cells. Dox is an anthracycline antibiotic, and its anticancer activity is widely known towards solid tumors like lung, breast, ovarian, thyroid and gastric cancers.[37]

For inhibition of cell growth testing, we first checked whether A549 cells alone or exposed to $POSP_m$ could be damaged under UV light irradiation at 365 nm with 430 mW/cm^2 for 20 min. Indeed, no significant difference in cell viability was found under UV light irradiation, and the cells maintained an intact morphology as compared with the control group (Supporting Information Figs. S6a & S6b). Subsequently, the cells were exposed to $POSP_m$@Dox at a relevant Dox concentration of 2 μg/mL, slightly larger than its IC_{50} value. Figure 7a shows 63.40 ± 7.36% and 47.33 ± 4.95% cell viabilities for the cells treated with free Dox and $POSP_m$@Dox respectively. The cells died significantly as exposed to $POSP_m$@Dox under UV light irradiation ($p < 0.05$, compared with free Dox or $POSP_m$@Dox). The relative cell viability was 16.75 ± 1.61%. The cellular uptake of Dox into the cells was traced by CLSM as well. Figure 7b shows the highest fluorescence intensity of Dox was observed in $POSP_m$@Dox with UV light irradiation, indicating that

the cleavage of ONB linkage indeed enhanced the drug release. The higher concentration of Dox released from $POSP_m$@Dox+UV also resulted in more serious damage of the cells. A distorted morphology of the cells is clearly seen in the DIC image.

Annexin-V/PI dual-staining assay was acquired for apoptosis testing. Consistent results were found as those observed by MTT assay (Figure 8a). The percentages of Annexin-V/PI staining positive cells (except lower left quadrant) are summed and plotted in Figure 8b, being 36.01 ± 4.66% for the cells treated with DOX, 43.90 ± 4.14% for the cells under UV irradiation, and 62.56 ± 3.18% for the cells with the combined treatment. Compared with free Dox and $POSP_m$@Dox, the significant increase in amount of death cells was found for $POSP_m$@Dox+UV.

■ CONCLUSION

A novel PCL-ONB-SS-PMAA diblock copolymer with photo- and redox-dual stimuli responsive sites adjacently located within the hydrophobic-hydrophilic core-shell junctions was successfully and firstly synthesized by –OH protection, de-protection method, ROP, and ATRP reactions. The stimuli-responsive degradable ability of the micelle was confirmed from TEM images, GPC profiles and UV-visible spectra. In *in vitro* studies, the micelle showed low cytotoxicity

against CRL-5802, A549 and HEL-299 cells. The intracellular uptake of the micelle was higher in A549 cells than in CRL5802 cells, and the internalization mechanism was mainly mediated by CME. The model drug Dox was efficiently encapsulated inside the core compartment of the micelle, and a synergistic Dox-released profile was found in the group with the treatment of GSH and UV light irradiation. This combination of redox- and photo-responsive cleavage behavior could enhance disintegration of the micelle in the tumor microenvironment. The highest released amount of Dox from $POSP_m$@Dox+UV showed the highest cell killing effect. Thus, this artificially-made micelle is promising for smart drug delivery.

■ CONFLICTS OF INTEREST

The authors declare that they have no conflict of interest.

■ ASSOCIATED CONTENT

The Supporting Information is available free of charge at https://pubs.acs.org

Synthetic procedures of PCL-ONB-ether-SS-PMAA, NMR spectra of synthesized compounds, GPC profiles, Critical aggregation concentration, NMR spectrum and TEM image after UV light irradiation, and Cell viability by MTT assay.

■ ACKNOWLEDGEMENTS

We are grateful for financial support from the Ministry of Science and Technology of Taiwan (grant nos. MOST106-2320-B-037-004-MY3 and MOST108-2221-B-037-002-MY3. This study was also supported by Kaohsiung Medical University under grant no. KMU-DK(個)109001, and by the NSYSU-KMU Joint Research Project under grant no. NSYSUKMU 109-P009. We appreciate the experimental support of a confocal laser scanning microscope and a transmission electron microscope provided by the Center for Research Resources and Development of Kaohsiung Medical University.

■ REFERENCES

(1) Fleige, E.; Quadir, M. A.; Haag, R., Stimuli-responsive polymeric nanocarriers for the controlled transport of active compounds: concepts and applications. *Adv. Drug Deliv. Rev.* **2012,** 64, 866-884.
(2) Cheng, R.; Meng, F.; Deng, C.; Klok, H. A.; Zhong, Z., Dual and multi-stimuli responsive polymeric nanoparticles for programmed site-specific drug delivery. *Biomaterials* **2013,** 34, 3647-3657.
(3) Zhang, Q.; Aleksanian, S.; Nohbc, S. M.; Oh, J. K., Thiol-responsive block

copolymer nanocarriers exhibiting tunable release with morphology changes. *Polym. Chem.-Uk* **2013,** 4, 351-359.

(4) Yu, M.; Zheng, J., Clearance pathways and tumor targeting of imaging nanoparticles. *ACS Nano* **2015,** 9, 6655-6674.

(5) Liu, G.; Liu, W.; Dong, C. M., UV- and NIR-responsive polymeric nanomedicines for on-demand drug delivery. *Polym. Chem.-Uk* **2013,** 4, 3431-3443.

(6) Aujard, I.; Benbrahim, C.; Gouget, M.; Ruel, O.; Baudin, J. B.; Neveu, P.; Jullien, L., *o*-Nitrobenzyl photolabile protecting groups with red-shifted absorption: syntheses and uncaging cross-sections for one- and two-photon excitation. *Chemistry (Easton)* **2006,** 12, 6865-6879.

(7) Marinzi, C.; Offer, J.; Longhi, R.; Dawson, P. E., An *o*-nitrobenzyl scaffold for peptide ligation: synthesis and applications. *Bioorg. Med. Chem.* **2004,** 12 (10), 2749-2757.

(8) Piggott, A. M.; Karuso, P., Synthesis of a new hydrophilic o-nitrobenzyl photocleavable linker suitable for use in chemical proteomics. *Tetrahedron Lett.* **2005,** 46, 8241-8244.

(9) Schade, B.; Hagen, V.; Schmidt, R.; Herbrich, R.; Krause, E.; Eckardt, T.; Bendig, J., Deactivation behavior and excited-state properties of (coumarin-4-yl)methyl derivatives. 1. Photocleavage of (7-methoxycoumarin-4-yl)methyl-caged acids with fluorescence enhancement. *J. Org. Chem.* **1999,** 64, 9109-9117.

(10) Beaute, L.; McClenaghan, N.; Lecommandoux, S., Photo-triggered polymer nanomedicines: From molecular mechanisms to therapeutic applications. *Adv. Drug Deliv. Rev.* **2019,** 138, 148-166.

(11) Cheng, R.; Feng, F.; Meng, F.; Deng, C.; Feijen, J.; Zhong, Z., Glutathione-responsive nano-vehicles as a promising platform for targeted intracellular drug and gene delivery. *J. Control. Release* **2011,** 152, 2-12.

(12) Huang, L.; Chaurasiya, B.; Wu, D.; Wang, H.; Du, Y.; Tu, J.; Webster, T. J.; Sun, C., Versatile redox-sensitive pullulan nanoparticles for enhanced liver targeting and efficient cancer therapy. *Nanomedicine* **2018,** 14, 1005-1017.

(13) Xuan, J.; Han, D.; Xia, H.; Zhao, Y., Dual-stimuli-responsive micelle of an ABC triblock copolymer bearing a redox-cleavable unit and a photocleavable unit at two block junctions. *Langmuir* **2014,** 30, 410-417.

(14) Huang, Q.; Liu, T.; Bao, C.; Lin, Q.; Ma, M.; Zhu, L., Light and reductive dual stimuli-responsive PEI nanoparticles: “AND” logic response and controllable release. *J. Mater. Chem. B* **2014,** 2, 3333-3339.

(15) Han, D.; Tong, X.; Zhao, Y., Block copolymer micelles with a dual-stimuli-responsive core for fast or slow degradation. *Langmuir* **2012,** 28 (5), 2327-2331.
(16) Cao, Z.; Zhou, X.; Wang, G., Selective release of hydrophobic and hydrophilic cargos from multi-stimuli-responsive nanogels. *ACS Appl. Mater. Inter.* **2016,** 8, 28888-28896.
(17) Han, D.; Tong, X.; Zhao, Y., Block copolymer micelles with a dual-stimuli-responsive core for fast or slow degradation. *Langmuir* **2012,** 28, 2327-2331.
(18) Zhang, P.; Zhang, H.; He, W.; Zhao, D.; Song, A.; Luan, Y., Disulfide-linked amphiphilic polymer-docetaxel conjugates assembled redox-sensitive micelles for efficient antitumor drug delivery. *Biomacromolecules* **2016,** 17, 1621-1632.
(19) Chen, J.; Qiu, X.; Ouyang, J.; Kong, J.; Zhong, W.; Xing, M. M., pH and reduction dual-sensitive copolymeric micelles for intracellular doxorubicin delivery. *Biomacromolecules* **2011,** 12, 3601-3611.
(20) Chan, N.; An, S. Y.; Oh, J. K., Dual location disulfide degradable interlayer-crosslinked micelles with extended sheddable coronas exhibiting enhanced colloidal stability and rapid release. *Polym. Chem.-Uk* **2014,** 5, 1637-1649.
(21) Liu, Y. S.; Huang, S. J.; Huang, X. S.; Wu, Y. T.; Chen, H. Y.; Lo, Y. L.; Wang, L. F., The synthesis and comparison of poly(methacrylic acid)–poly(ε-caprolactone) block copolymers with and without symmetrical disulfide linkages in the center for enhanced cellular uptake. *RSC Adv.* **2016,** 6, 75092-75103.
(22) Li, W.; Wang, J.; Ren, J.; Qu, X., Near-infrared upconversion controls photocaged cell adhesion. *J. Am. Chem. Soc.* **2014,** 136, 2248-2251.
(23) Bertrand, O.; Poggi, E.; Gohy, J. F.; Fustin, C. A., Functionalized stimuli-responsive nanocages from photocleavable block copolymers. *Macromolecules* **2014,** 47, 183-190.
(24) Lee, J. E.; Ahn, E.; Bak, J. M.; Jung, S. H.; Park, J. M.; Kim, B. S.; Lee, H. I., Polymeric micelles based on photocleavable linkers tethered with a model drug. *Polymer* **2014,** 55, 1436-1442.
(25) Lee, R. S.; Li, Y. C.; Wang, S. W., Synthesis and characterization of amphiphilic photocleavable polymers based on dextran and substituted-ε-caprolactone. *Carbohydr. Polym.* **2015,** 117, 201-210.
(26) Jalani, G.; Naccache, R.; Rosenzweig, D. H.; Haglund, L.; Vetrone, F.; Cerruti, M., Photocleavable hydrogel-coated upconverting nanoparticles: A multifunctional theranostic platform for NIR imaging and on-demand macromolecular delivery. *J. Am. Chem. Soc.* **2016,** 138, 1078-1083.

(27) Zhao, H.; Sterner, E. S.; Coughlin, E. B.; Theato, P., o-Nitrobenzyl alcohol derivatives: opportunities in polymer and materials science. *Macromolecules* **2012,** 45, 1723-1736.

(28) Lo, Y. L.; Chou, H. L.; Liao, Z. X.; Huang, S. J.; Ke, J. H.; Liu, Y. S.; Chiu, C. C.; Wang, L. F., Chondroitin sulfate-polyethylenimine copolymer-coated superparamagnetic iron oxide nanoparticles as an efficient magneto-gene carrier for microRNA-encoding plasmid DNA delivery. *Nanoscale* **2015,** 7, 8554-8565.

(29) Liu, Y. S.; Chiu, C. C.; Chen, H. Y.; Chen, S. H.; Wang, L. F., Preparation of chondroitin sulfate-g-poly(epsilon-caprolactone) copolymers as a CD44-targeted vehicle for enhanced intracellular uptake. *Mol. Pharm.* **2014,** 11, 1164-1175.

(30) Harush-Frenkel, O.; Debotton, N.; Benita, S.; Altschuler, Y., Targeting of nanoparticles to the clathrin-mediated endocytic pathway. *Biochem. Biophys. Res. Commun.* **2007,** 353, 26-32.

(31) Li, W.; Chen, C.; Ye, C.; Wei, T.; Zhao, Y.; Lao, F.; Chen, Z.; Meng, H.; Gao, Y.; Yuan, H.; Xing, G.; Zhao, F.; Chai, Z.; Zhang, X.; Yang, F.; Han, D.; Tang, X.; Zhang, Y., The translocation of fullerenic nanoparticles into lysosome via the pathway of clathrin-mediated endocytosis. *Nanotechnology* **2008,** 19, 145102.

(32) Rappoport, J. Z., Focusing on clathrin-mediated endocytosis. *Biochem. J.* **2008,** 412, 415-423.

(33) Smith, P. J.; Giroud, M.; Wiggins, H. L.; Gower, F.; Thorley, J. A.; Stolpe, B.; Mazzolini, J.; Dyson, R. J.; Rappoport, J. Z., Cellular entry of nanoparticles via serum sensitive clathrin-mediated endocytosis, and plasma membrane permeabilization. *Int J Nanomedicine* **2012,** 7, 2045-2055.

(34) Chen, G. J.; Hsu, C.; Ke, J. H.; Wang, L. F., Imaging and chemotherapeutic comparisons of iron oxide nanoparticles chemically and physically coated with poly(ethylene glycol)-*b*-poly(*ε*-caprolactone)-*g*-poly(acrylic acid). *J. Biomed. Nanotech.* **2015,** 11, 951-963.

(35) Bae, Y. H.; Park, K., Targeted drug delivery to tumors: myths, reality and possibility. *J. Control. Release* **2011,** 153, 198-205.

(36) Spain, S. G.; Cameron, N. R., A spoonful of sugar: the application of glycopolymers in therapeutics. *Polym Chem-Uk* **2011,** 2, 60-68.

(37) Tacar, O.; Sriamornsak, P.; Dass, C. R., Doxorubicin: an update on anticancer molecular action, toxicity and novel drug delivery systems. *J. Pharm. Pharmacol.* **2013,** 65, 157-170.

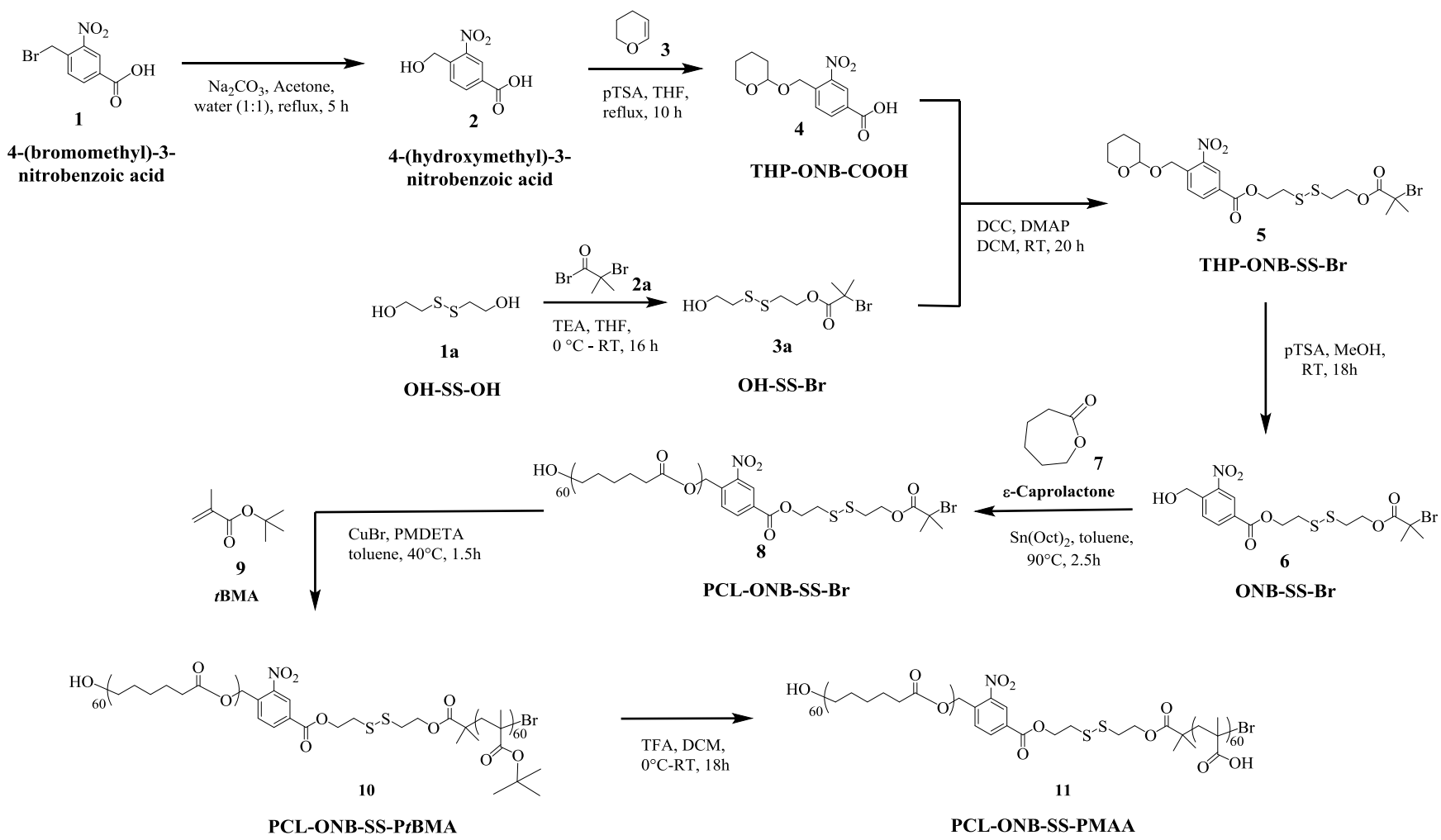

Scheme 1. Synthetic procedures of amphiphilic block copolymer PCL-ONB-SS-PMAA (POSP)

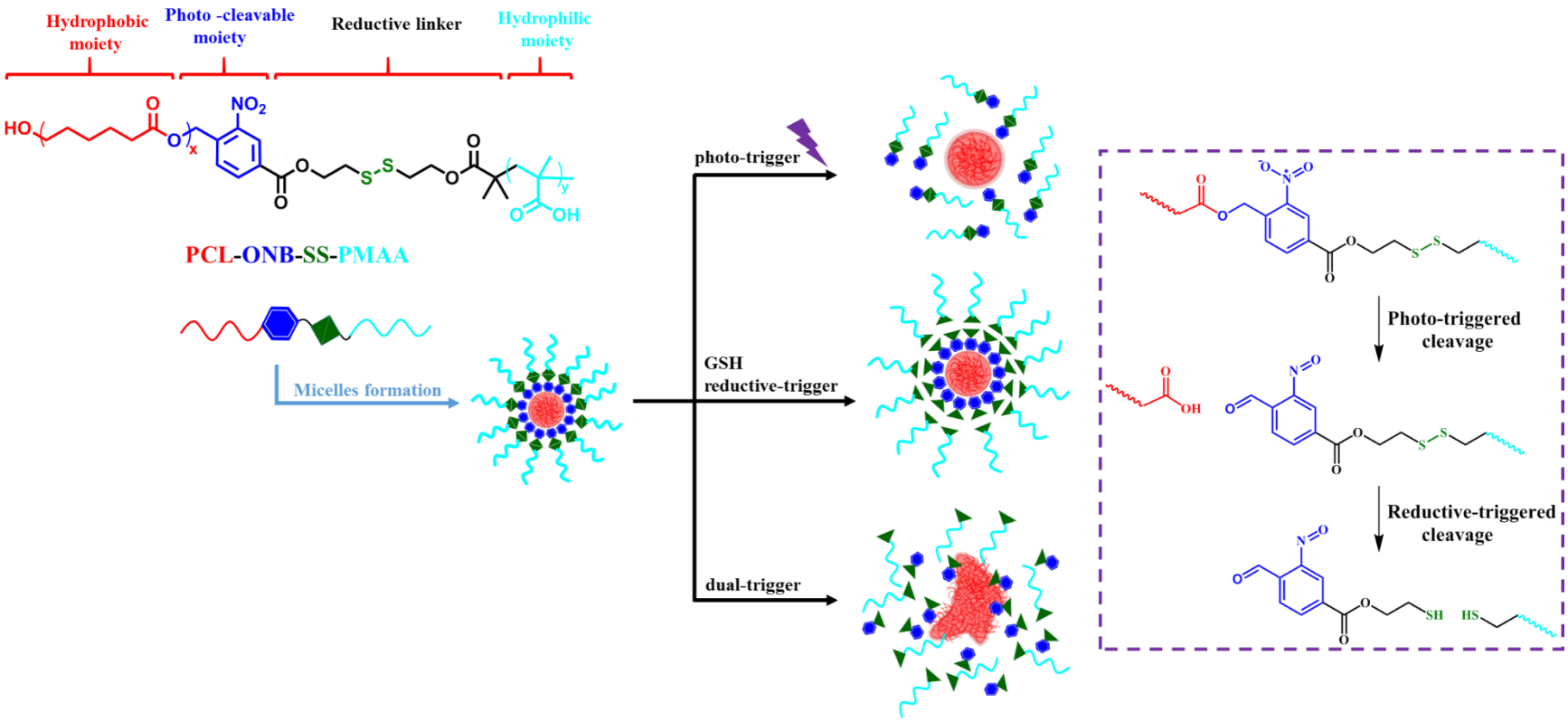

Scheme 2. Illustration of POSP-formed micelle ($POSP_m$) triggered by photo and GSH dual-responsive degradation.

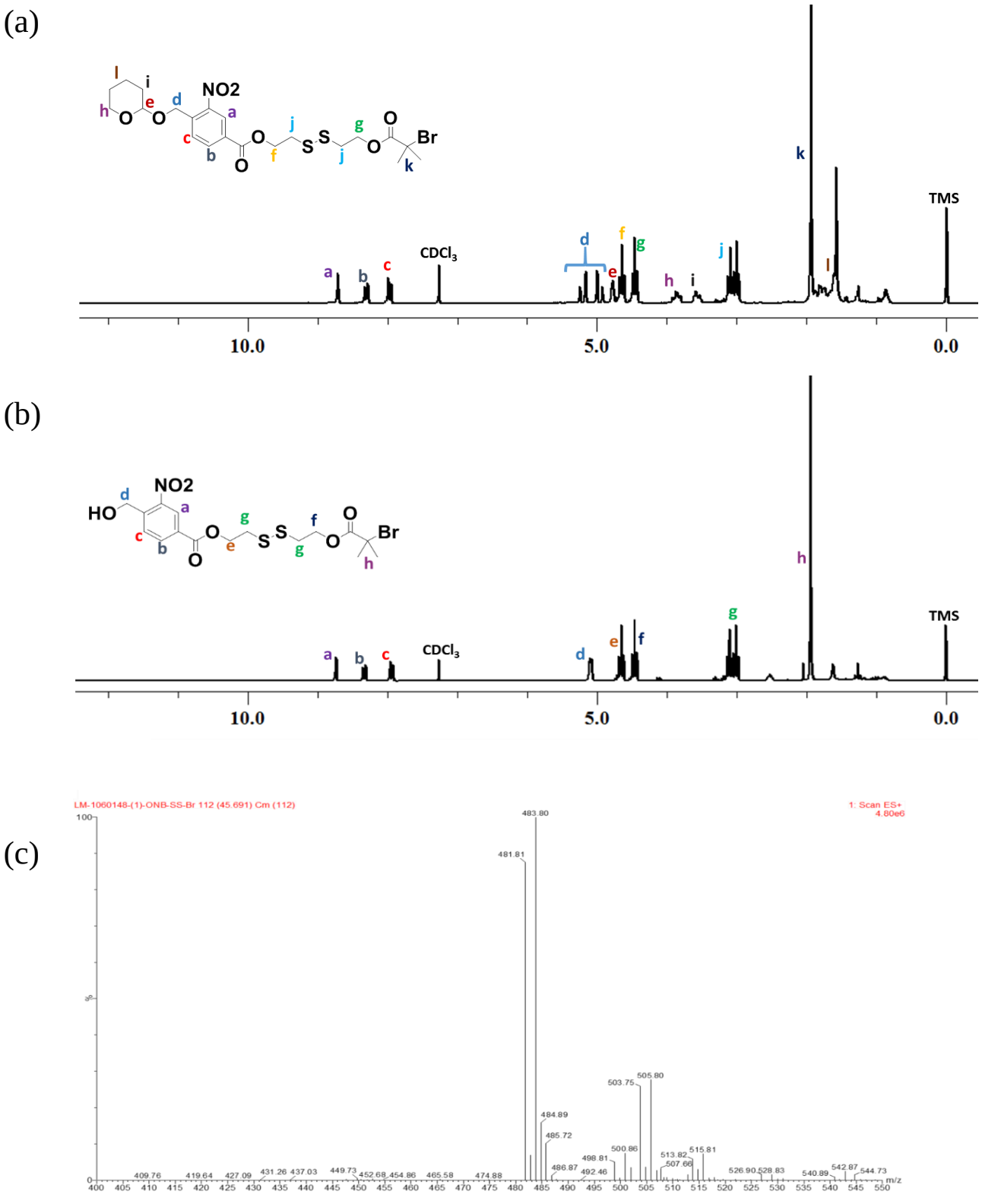

Figure 1. Characterization of HO-ONB-SS-Br macroinitiator. (a) NMR spectrum of THP-ONB-SS-Br. (b) NMR spectrum and (c) LC/MS spectrum of HO-ONB-SS-Br.

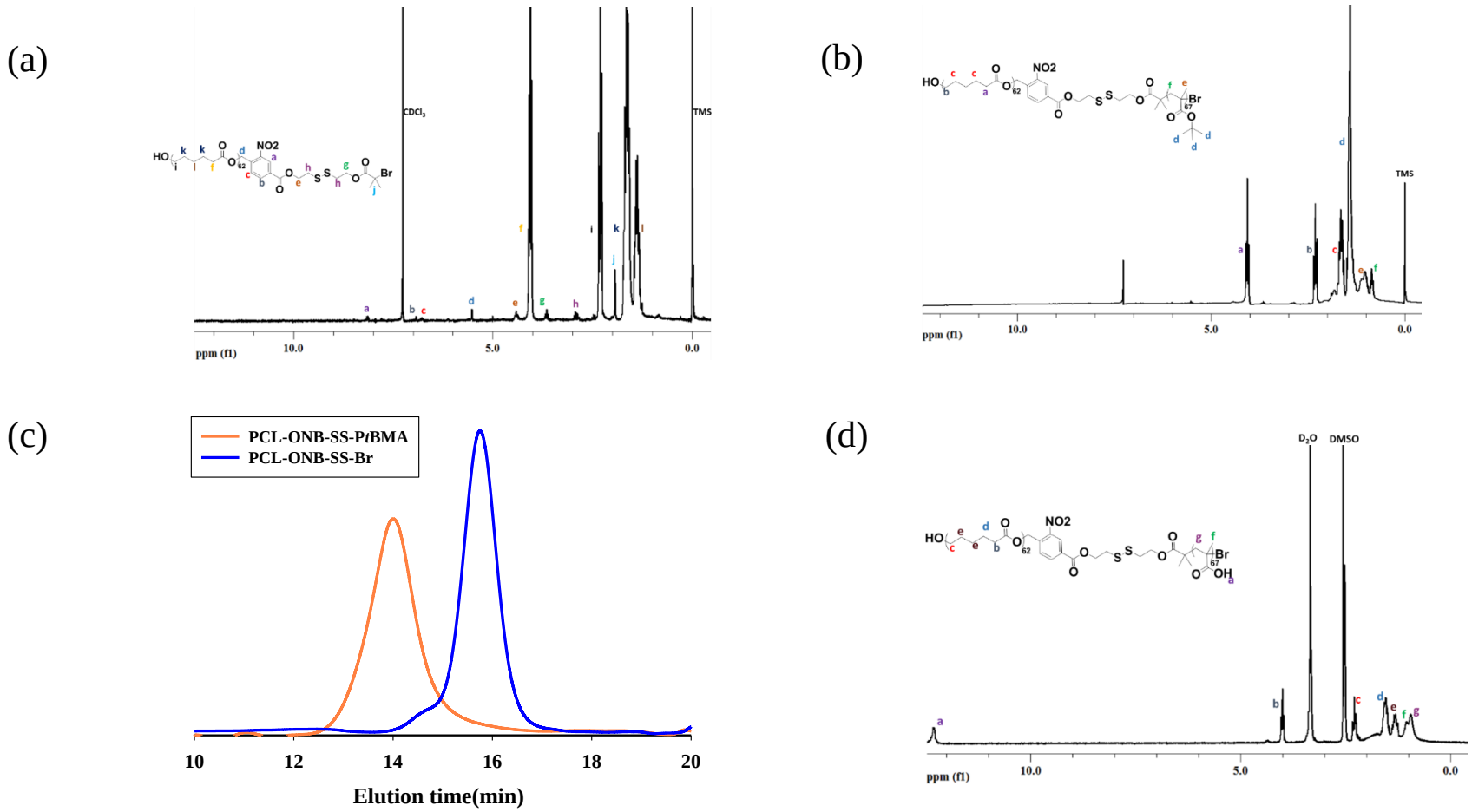

Figure 2. Characterization of PCL-ONB-SS-PMAA. (a) NMR spectrum of PCL-ONB-SS-Br; (b) NMR spectrum of PCL-ONB-SS-P*t*BMA; (c) GPC diagram of PCL-ONB-SS-Br and PCL-ONB-SS-P*t*BMA; (d) NMR spectrum of PCL-ONB-SS-PMAA.

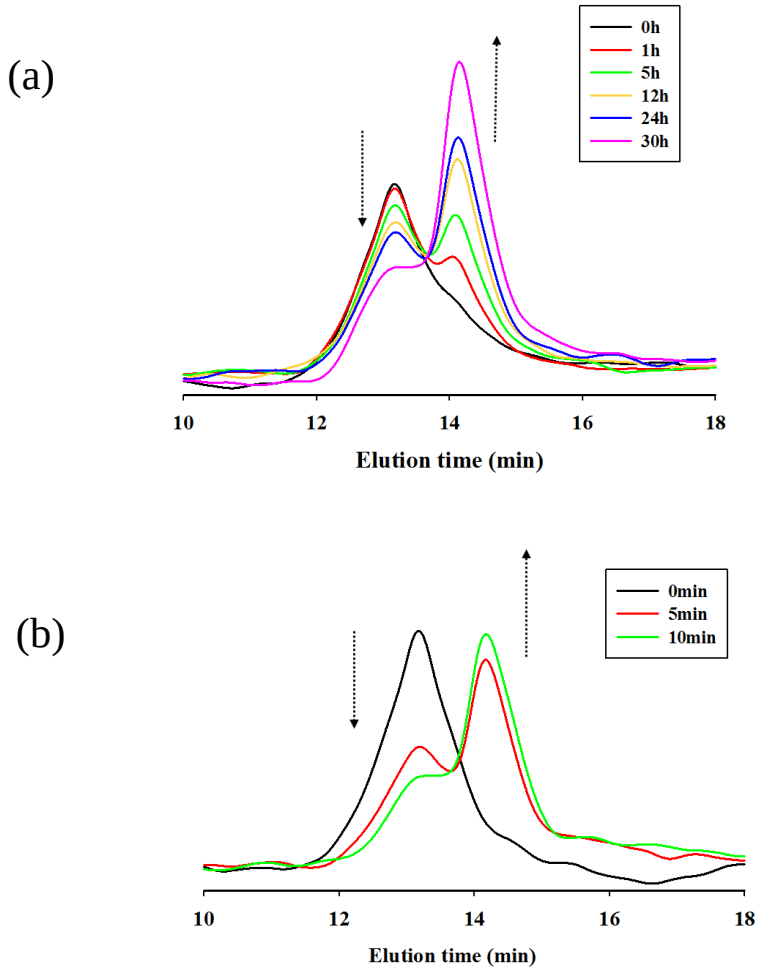

Figure 3. Dual response of PCL-ONB-SS-P*t*BMA. (a) GPC profiles of PCL-ONB-SS-P*t*BMA in THF treated with 50 mM DTT (Dithiothreitol) for various time periods. (b) GPC profiles of PCL-ONB-SS-P*t*BMA in THF under UV light irradiation (365 nm, 430 mW/cm^2) for 0, 5 and 10 min.

(a)

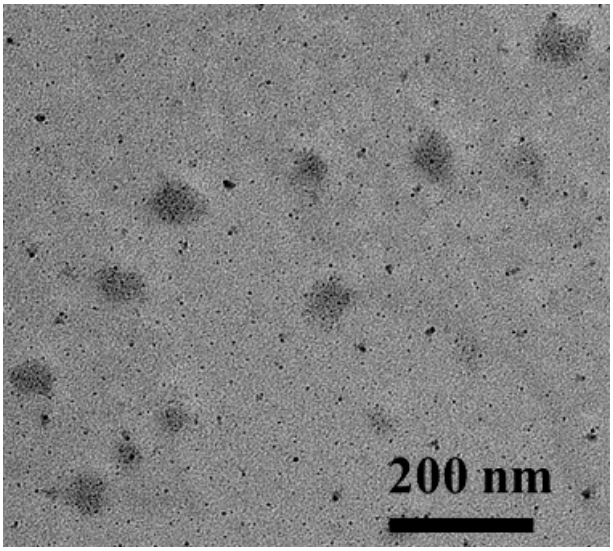

(b)

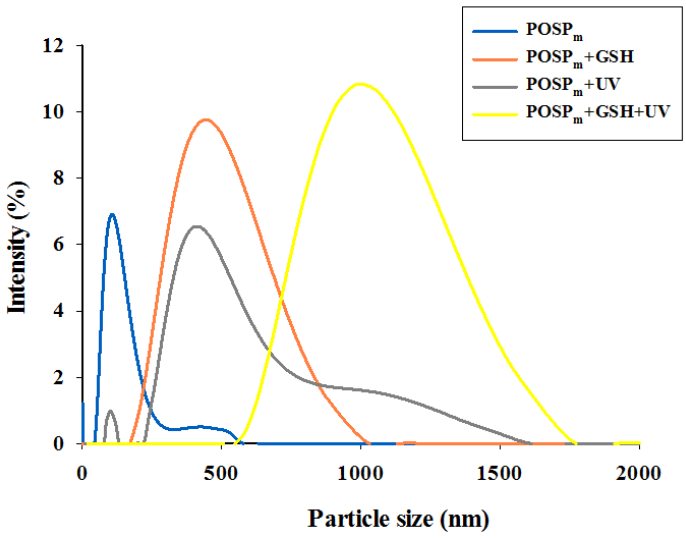

Figure 4. Morphology of PCL-ONB-SS-PMAA-formed micelle ($POSP_m$) and changes of size distribution of $POSP_m$ with different stimuli. (a) A TEM image of $POSP_m$. (b) Change of size distribution profiles of $POSP_m$ treated with 10 mM GSH for 20 min, UV light irradiation for 20 min (365 nm, 430 mW/cm^2) and both combined.

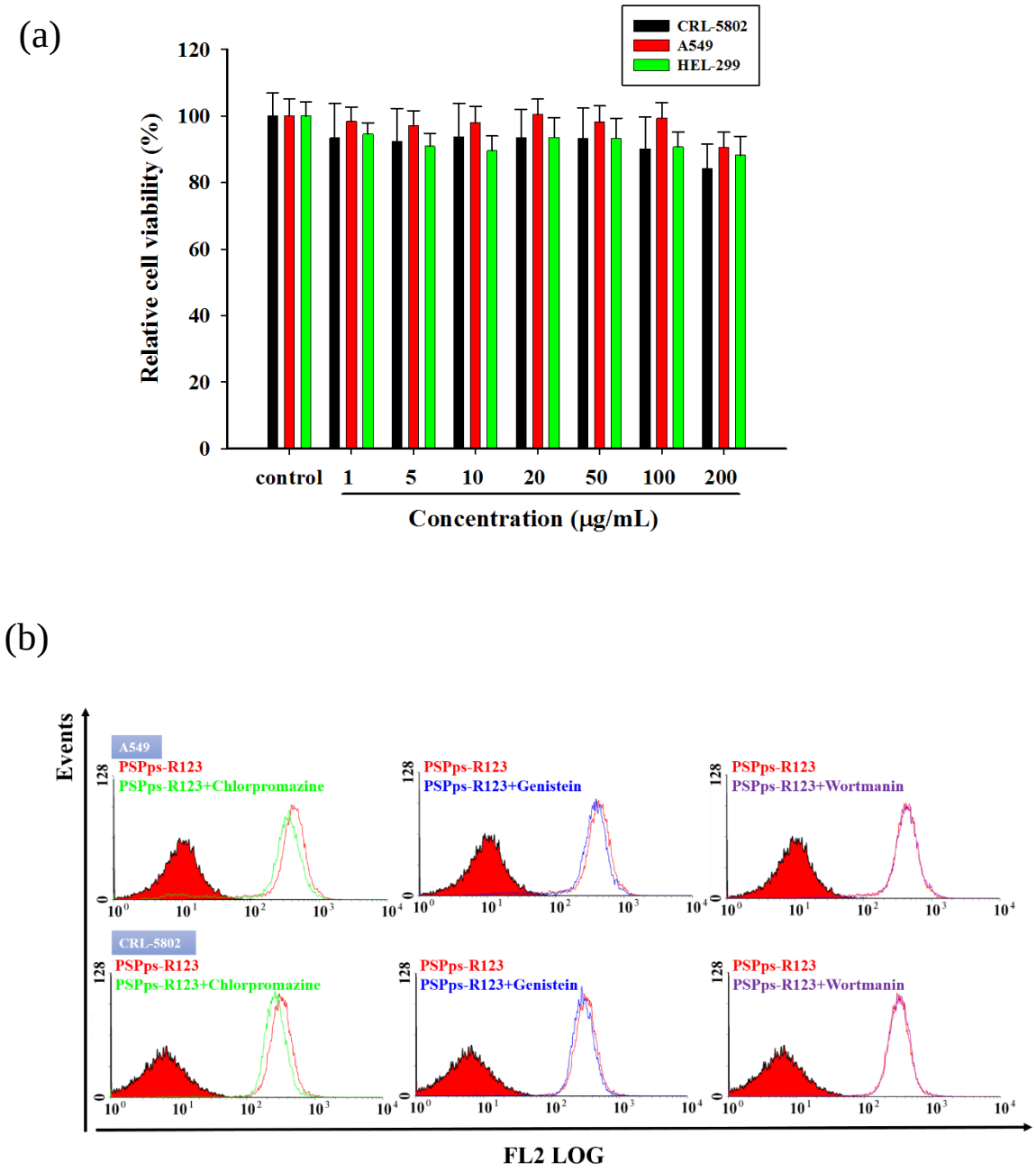

Figure 5. Cytotoxicity and internalization pathway of the micelle. (a) Relative cell viability of CRL-5802, A549, and HEL-299 cells exposed to various concentrations of $POSP_m$. (b) Flow cytometry diagrams of CRL-5802 cells and A549 cells exposed to rhodamine-123 (R123)-conjugated $POSP_m$ at a concentration of 100 μg/mL for 4 h incubation. Cells were pretreated with different chemical inhibitors: 10 $\mu g \cdot mL^{-1}$ chlorpromazine, 200 μM genistein and 50 nM wortmannin for 30 min.

(a)

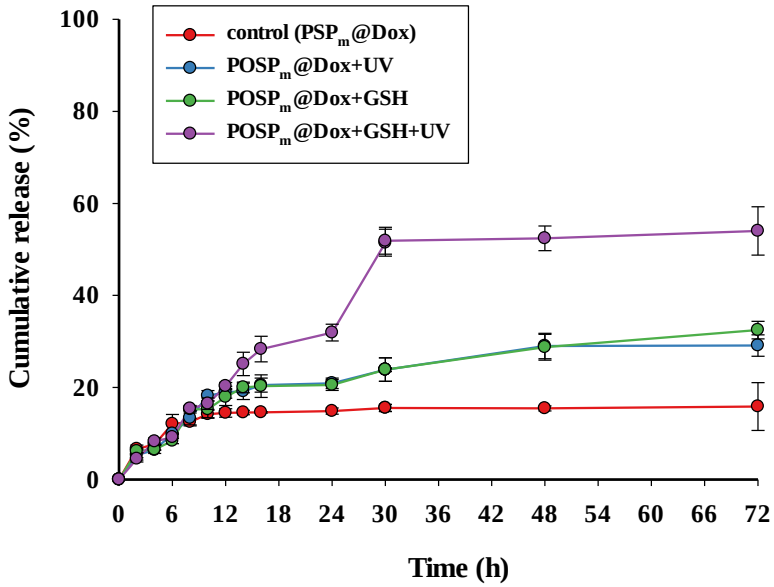

(b)

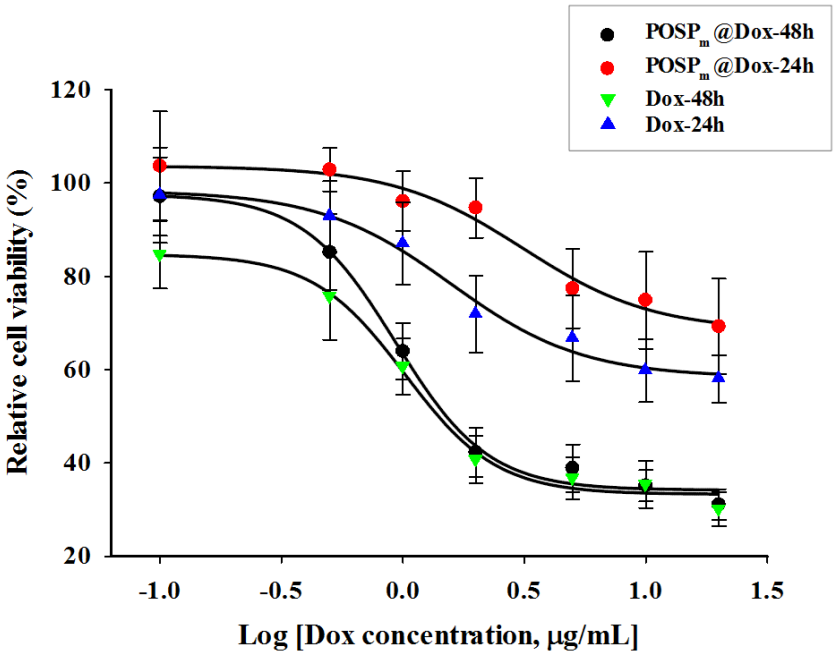

Figure 6. Drug release and cytotoxicity of POSP$_m$@Dox. (a) *In vitro* Dox release profiles of POSP$_m$@Dox with different treatments. Control means the POSP$_m$@Dox solution was dialyzed against 10 mL of PBS at pH 7.4; POSP$_m$@Dox+UV means the dialyzed solution was irradiated by UV light at the time points of 6 h, 12 h and 24 h; POSP$_m$@Dox+GSH means the solution was dialyzed against PBS at pH 7.4 containing 10 mM GSH after 6 h; POSP$_m$@Dox+GSH+UV means the solution was dual treated with GSH and UV light at 6, 12 and 24 h, respectively (n = 4). (b) Relative cell viability of POSP$_m$@Dox and free Dox against A549 cells for 24 and 48 h postincubation. (n = 8)

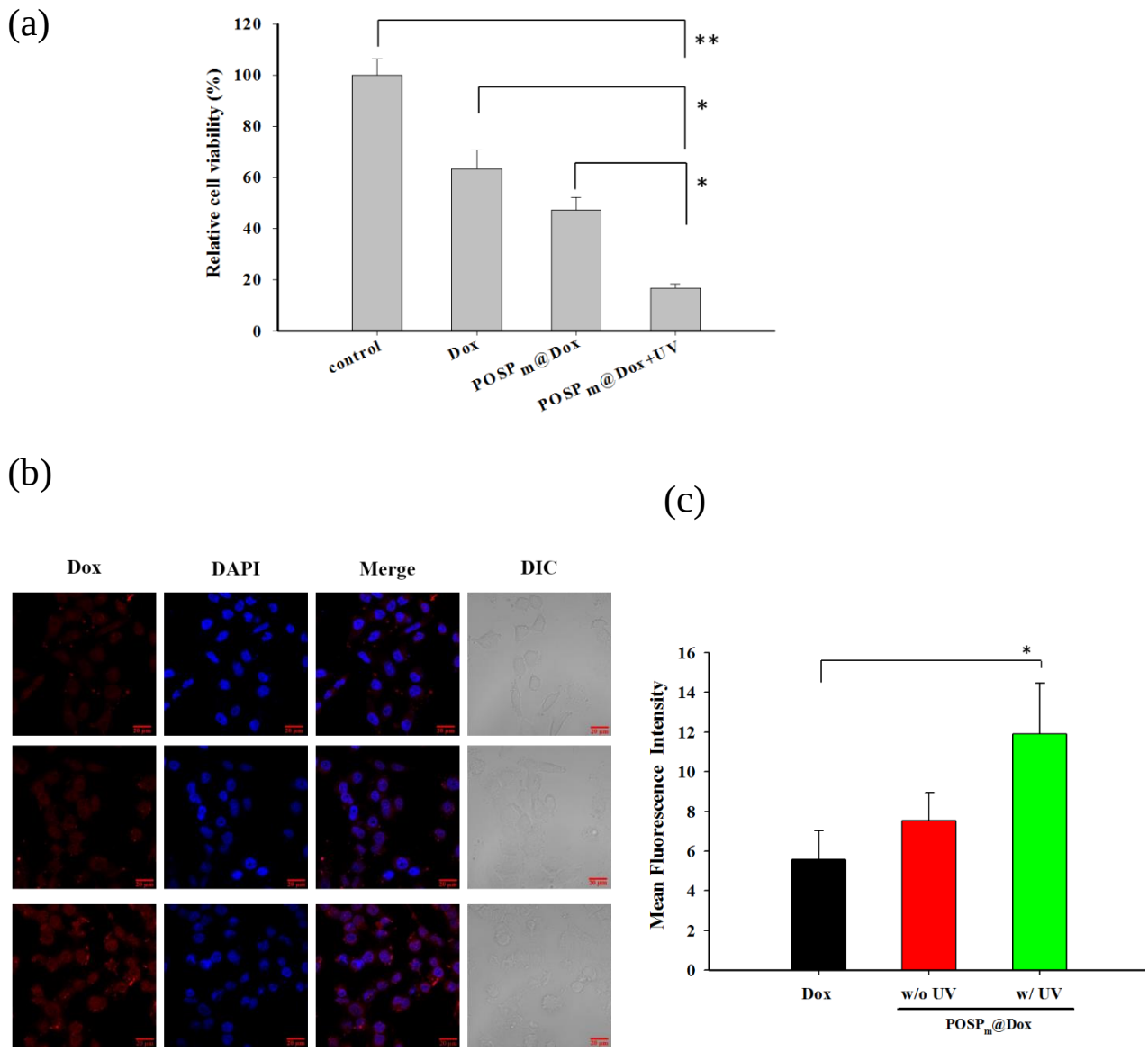

Figure 7. **Cytotoxicity and CLSM images of test samples.** (a) Relative cell viability of A549 cells exposed to an equivalent Dox concentration of $POSP_m$@Dox at 2 μg/mL for 48 h postincubation with or without UV irradiation (365 nm, 430 mW/cm^2) for 20 min (n = 8, *p < 0.05, **p < 0.01). (b) Confocal images of A549 cells exposed to free Dox and $POSP_m$@Dox for 4 h with or without UV irradiation for 20 min. Red: fluorescence of Dox, Blue: nuclei stained by DAPI. Scale bar is 20 μm. (c) Mean fluorescence intensity analyzed by MetaVue software (n = 10, *p < 0.05).

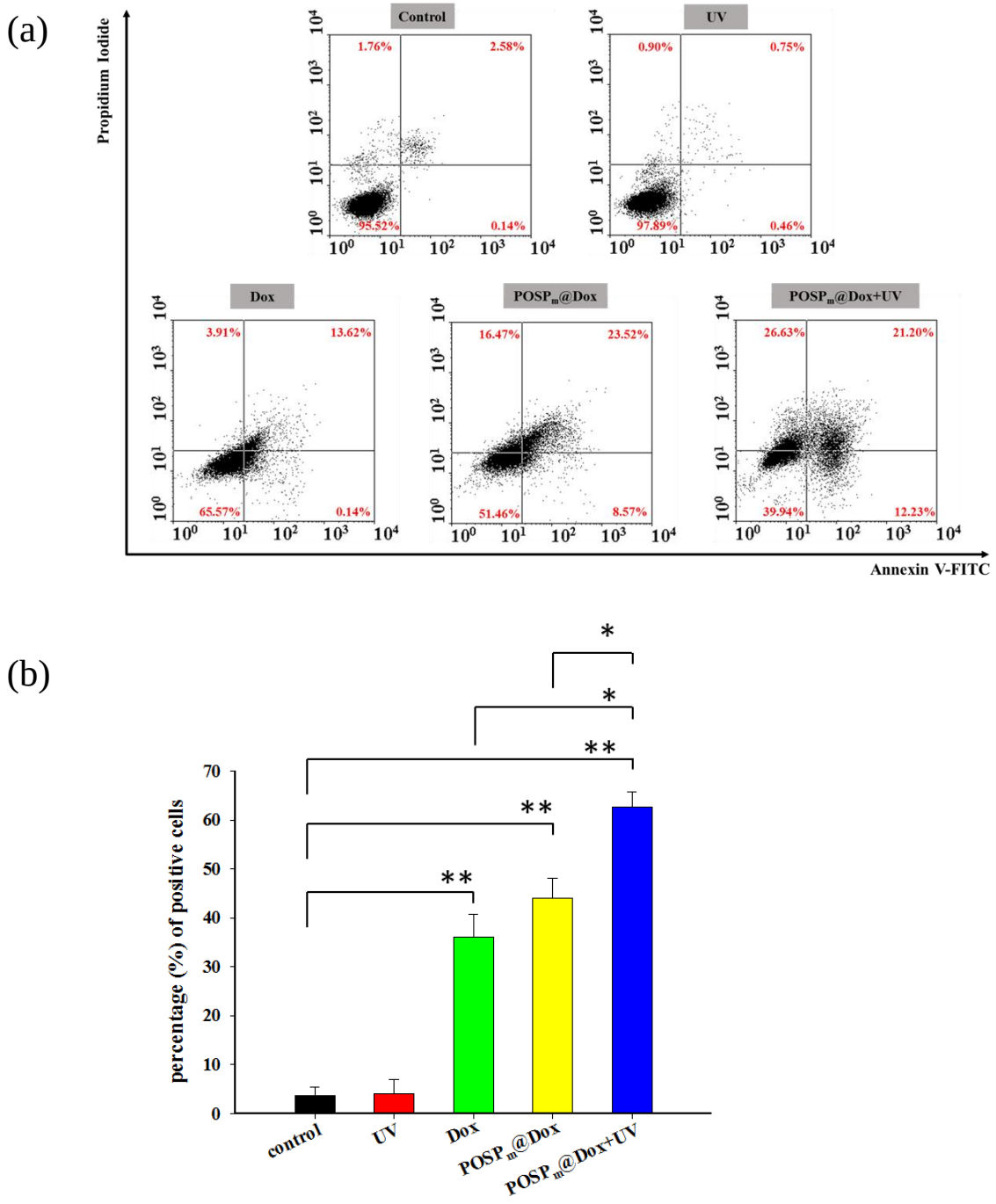

Figure 8. Cell apoptosis of test samples. (a) Annexin-V/PI (propidium iodide) dual-staining assay for apoptosis by flow cytometry analysis. A549 cells exposed to free Dox or $POSP_m$@Dox (the equivalent Dox concentration was fixed at 2 μg/mL) with or without UV irradiation. Following 4 h incubation, all samples were replaced with fresh media. The UV light was applied at 365 nm and 430 mW/cm^2 for 20 min. (b) Percentage of Annexin-V/PI staining positive cells (except lower left quadrant) was plotted based on the results obtained from (a). (n = 3, *$p < 0.05$, **$p < 0.01$)

Graphic Table of Contents